Reduced Graphene Oxide Membranes for Ultrafast Organic Solvent Nanofiltration

*Liang Huang, Ji Chen, Tiantian Gao, Miao Zhang, Yingru Li, Liming Dai, Liangti Qu, and Gaoquan Shi**

Chemical and pharmaceutical industries often involve chemical and biochemical syntheses requiring the separation or purification of their products from organic media and/or under harsh chemical environments. The traditional separation and purification techniques (e.g., evaporation and distillation) are usually energy-intensive and need large spaces, making the separation processes account for 40%–70% of both capital and operating costs.[1] In contrast, membrane-based separations can be carried out under mild conditions, which is cheap, convenient, environmentally friendly, and space saving.[1,2] For practical applications in dealing with a large volume of organic solution, the organic solvent nanofiltration (OSN) membranes must be stable in organic solvents and have high solvent permeances to save processing time.[1,2] However, because of their thick densified separating layers, commercially available polymeric or ceramic OSN membranes are still insufficiently permeable to satisfy industrial demands for filtrating large volumes of organic solvents.[1–4] To achieve a high solvent permeance, the separating layer of an OSN membrane should be as thin as possible without sacrificing their mechanical strength or inducing defects such as pinholes and cracks.[3,4] Recently, freestanding diamond-like carbon membranes (35 nm thick) and polyamide films (<10 nm in thickness) were explored as effective separating layers,[3,4] and the polyamide OSN membranes exhibited high retentions of solutes with an unprecedented acetone permeance of about 50 liters per square meter per hour per bar (L m^{-2} h^{-1} bar^{-1}).[3]

On the other hand, reduced graphene oxide (rGO) is an atom-thick 2D carbon nanomaterial, exhibiting excellent tolerance to organic solvents and harsh chemical environments.[5,6] Furthermore, rGO sheets are dispersible in water, and they are unique building blocks for preparing self-assembled ultrathin membranes with a layered structure.[6] The 2D nanochannels between adjacent rGO layers can be used as 2D passages for molecules smaller than the thicknesses of nanochannels, while blocking the larger species (**Figure 1**a).[7–9] The narrow size distribution of rGO nanochannels provides them with better performances in precise molecular sieving than those of commonly used polymeric membranes.[10] Recently, Huang et al. reported the fast and selective water transport through GO composite membranes.[11,12] Unfortunately, GO membranes are unstable in water or under harsh chemical conditions.[13,14] Ultrathin membranes based on rGO have also been extensively explored for water purification, showing high water fluxes.[15–21] However, the permeances of rGO or GO membranes for organic solvents were tested to be extremely low; less than 7.5 L m^{-2} h^{-1} bar^{-1} for acetone.[22,23]

Here, we report ultrafast OSN membranes prepared by depositing ultrathin layers of solvent solvated rGO (S-rGO) onto commercially available microfiltration membranes. Typically, the OSN membrane with 18 nm thick S-rGO coating showed an acetone permeance as high as 215 L m^{-2} h^{-1} bar^{-1}. This membrane is also stable to organic solvents (e.g., methanol, acetone, and dimethylformamide), and even to strong acidic (e.g., sulfuric acid), alkaline (e.g., potassium hydroxide), or oxidative (e.g., nitric acid) media. The pristine S-rGO coating is negatively charged because of ionization of its residual carboxyl groups,[6] exhibiting high rejection to small molecules with negative charges. Neutral solutes with molecular sizes larger than the thickness of nanochannels in S-rGO (about 3.4 nm) can also be completely rejected. By functionalizing the S-rGO membrane with hyperbranched poly(ethylene imine) (HPEI) to switch its surface charge to be positive, small solute molecules (e.g., 1.6 nm) with positive charges can also be rejected.

Graphene oxide (GO) was prepared by a modified Hummers method[24] and it was reduced with hydrazine to form an aqueous dispersion (Figure S1, Supporting Information).[6] The as-prepared rGO dispersion was vacuum filtrated through a Nylon or anodic aluminum oxide (AAO) microfiltration membrane. The pore size of Nylon microfiltration membrane is about 0.65 μm (or 0.20 μm for AAO) (Figure 1b), smaller than the average lateral dimension of rGO sheets (≈2 μm, Figure S2, Supporting Information). As a result, rGO sheets were deposited onto the surface of microfiltration membrane to form a uniform coating (Figure 1c and Figure S3, Supporting Information). The filtration process was stopped as the rGO dispersion in filter disappeared, while the membrane was still wet. The wet composite membrane was immediately soaked in an organic solvent or water to keep its solvated state (Figure S4, Supporting Information), and it was nominated as S-rGO-*n* membrane (*n* is the thickness of S-rGO coating in nanometer). If the S-rGO coating was completely dried, rGO sheets would

L. Huang, J. Chen, T. T. Gao, M. Zhang, Y. R. Li,
Prof. G. Q. Shi
Department of Chemistry
Tsinghua University
Beijing 100084, P. R. China
E-mail: gshi@tsinghua.edu.cn
Prof. L. M. Dai
Center of Advanced Science and Engineering for Carbon (Case 4carbon)
Department of Macromolecular Science and Engineering
Case Western Reserve University
10900 Euclid Avenue, Cleveland OH 44106, USA
Prof. L. T. Qu
School of Chemistry
Beijing Institute of Technology
Beijing 100081, P. R. China

DOI: 10.1002/adma.201601606

ADVANCED MATERIALS
www.advmat.de

www.MaterialsViews.com

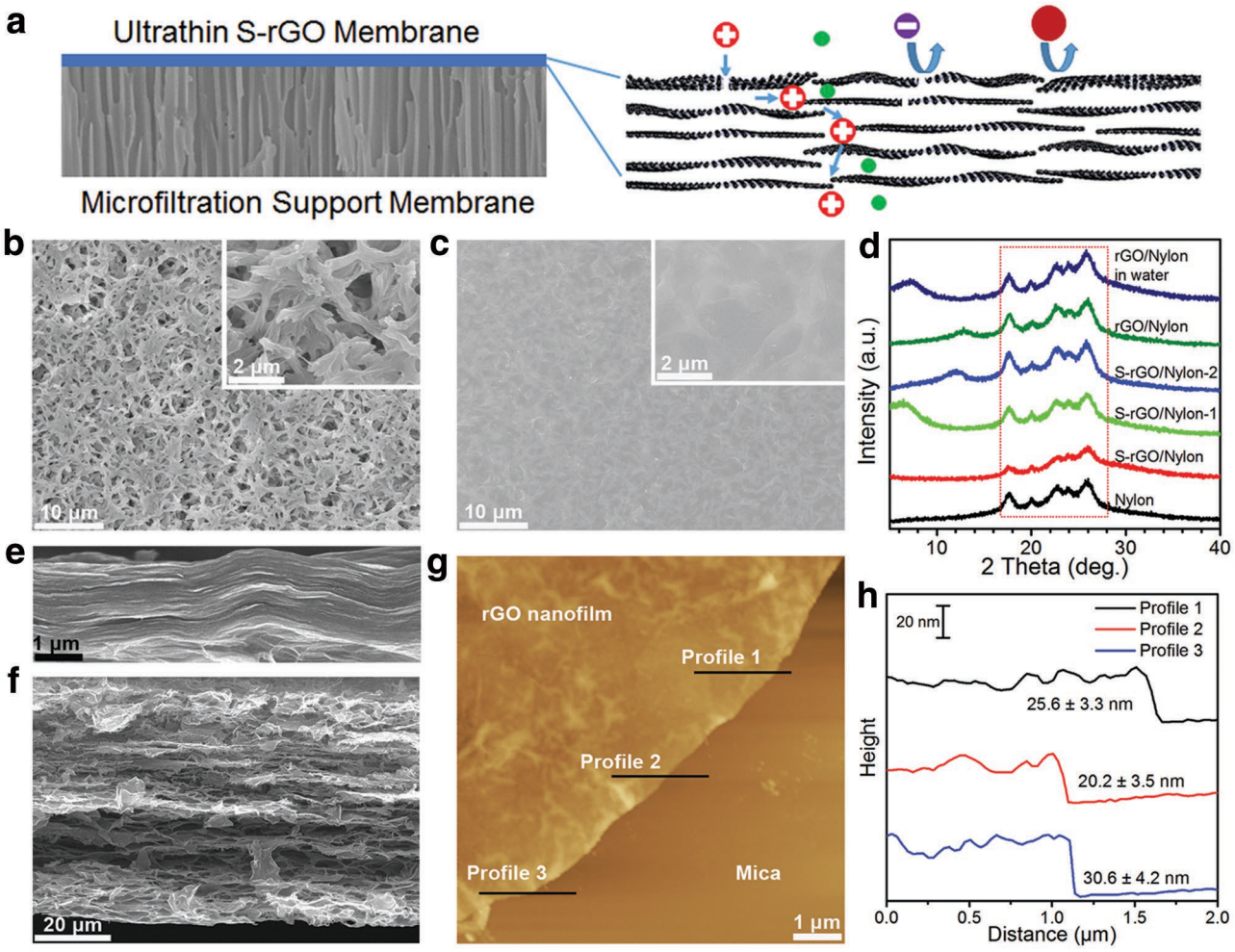

Figure 1. The structure of an S-rGO-*n* membrane and its molecular separation mechanism. a) Schematic illustration of depositing an ultrathin negatively charged S-rGO coating on the surface of a microfiltration support membrane, and the separation mechanism for charged solutes (electrostatic repulsion) and/or big neutral molecules (size exclusion). The SEM images of a microfiltration membrane b) before and c) after the deposition of an S-rGO coating. d) The evolution of XRD patterns of an S-rGO/Nylon membrane upon drying in air; S-rGO/Nylon-1 and S-rGO/Nylon-2 refer to the S-rGO/Nylon membrane dried for 3 and 5 min. The cross-sectional SEM image of e) an air-dried rGO membrane and f) a freeze-dried S-rGO membrane. g,h) AFM image and corresponding height profiles of an air-dried S-rGO film with mass loading of 44.09 mg m^{-2} on a mica sheet.

irreversibly restack to form a more ordered compact microstructure. This fact has been confirmed by X-ray diffraction (XRD) examinations. The XRD pattern of an S-rGO-*n* membrane showed only the diffraction peaks of its underneath Nylon support (Figure 1d) without any diffraction peaks related to stacked rGO sheets at $2\theta < 16°$. In comparison, during the process of drying in air, a peak associated with stacked rGO sheets between $2\theta = 5–13°$ gradually appeared. For example, after drying in air for 3 min, S-rGO/Nylon-1 showed an XRD peak at $2\theta = 6°$ (Figure 1d). With the elongation of drying time (e.g., 5 min), this peak shifted to larger angles (e.g., $2\theta = 12°$) and finally stabilized at $2\theta = 13°$ as this composite membrane was completely dried (named as rGO/Nylon). These results indicate that the S-rGO coating transformed into a more compact microstructure during the drying process. This structural change is irreversible. As can be seen from Figure 1d, after soaking in water for a day, the XRD pattern of rGO/Nylon still cannot be recovered to its original solvated state (S-rGO/Nylon).

The structural difference between dry rGO and S-rGO coatings has also been characterized by scanning electron microscope (SEM). A freeze-dried S-rGO film (≈80 μm) was measured to be much thicker than an air-dried counterpart (≈2 μm) with the same rGO loading of 4.19 g m^{-2} (Figure S5, Supporting Information), reflecting that the former has a more loosely stacking microstructure as confirmed also by the cross-sectional SEM images shown in Figure 1e,f. The S-rGO coating of an S-rGO-*n* membrane was detached from its AAO support by HCl etching and transferred onto a mica sheet for measuring its thickness by atomic force microscope (AFM). The S-rGO coating with an rGO loading of 44.09 mg m^{-2} has a thickness of about 25 nm (Figure 1g,h). This thickness can be further reduced to 18 nm by coating only 33.08 mg m^{-2} of rGO (S-rGO-18). Further reducing the loading of rGO led to the formation of defective membranes with cracks and pinholes (Figure S6, Supporting Information), exhibiting a poor molecular selectivity.

Adv. Mater. **2016**,
DOI: 10.1002/adma.201601606

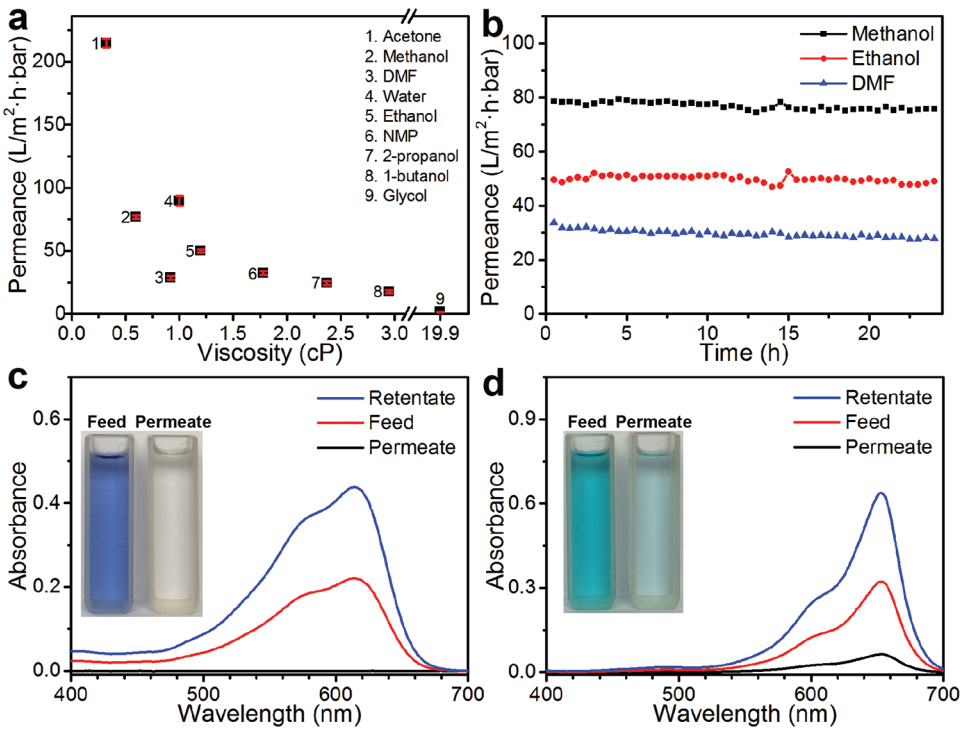

Figure 2. Nanofiltration performances of S-rGO-18 and HPEI/S-rGO-18 membranes. a) Plot of solvent permeance versus the viscosity of solvent and b) the variations of solvent permeances with time for S-rGO-18 membranes. c) Ultraviolet–visible (UV–vis) absorption spectra of a methanol solution of EB before and after filtration through an S-rGO-18 membrane; inset shows the photographs of the feed and permeate of EB solution. d) UV–vis absorption spectra of a methanol solution of MB before and after filtration through an HPEI/S-rGO-18 membrane; inset shows the photographs of the feed and permeate of the MB solution.

The stable solvent permeances of various solvents through an S-rGO-18 membrane were studied by using a stirred filtration setup (Figure S7 and S8, Supporting Information). Compared with a dry rGO composite membrane with the same mass loading of rGO (33.08 mg m^{-2}), S-rGO-18 membrane exhibited much higher (more than 10 times) solvent permeances because of its solvent solvated microstructure. **Figure 2**a plots the permeances of different solvents versus their viscosities. Accordingly, S-rGO-18 membrane has an unprecedentedly high permeance of 215 L m^{-2} h^{-1} bar^{-1} for acetone because of its porous microstructure and the low viscosity of this solvent (0.32 centipoise, cP). This value is about two orders of magnitude higher than that of currently commercialized OSN membranes (≈2.5 L m^{-2} h^{-1} bar^{-1}).[1,2] However, for 2-propanol, an organic solvent with molecular size comparable to that of acetone, the permeance of solvent decreased to 24 L m^{-2} h^{-1} bar^{-1} because of its much higher viscosity (2.37 cP). In general, the solvent permeance through an OSN membrane is determined by the viscosity and molecular size of the solvent, as well as the interaction between solvent molecules and membrane.[3] In our case, the viscosity of solvent was demonstrated to be the dominating factor (Figure 2a,b). However, solvent permeance is not inversely proportional to viscosity; thus, the other two factors should also have contributions. The solvent permeance of an S-rGO-*n* membrane strongly depends on the thickness of its S-rGO coating. A thicker S-rGO coating led to a lower solvent permeance (Figure S9, Supporting Information) because of its longer channel tortuosity. The solvent permeance increased linearly with applied pressure in the range from 1.0 to 5.0 bar (Figure S9, Supporting Information), reflecting the nanochannels of S-rGO separating layer kept unchanged upon compression.

Molecular selectivity is another important parameter for evaluating the performance of a nanofiltration membrane.[1,2] Dye molecules were usually used as molecular probes to characterize the selectivity of a nanofiltration membrane because of their easy detection, good solubility, and broad choice.[1] Thus, we selected a series of dye molecules with different sizes and charges for this purpose, and their chemical structures are illustrated in Figure S10 (Supporting Information). The typical S-rGO-18 membrane is negatively charged as described above, completely rejecting negatively charged Evans blue molecules (EB, 960.8 g mol^{-1}, 3.4 nm) from methanol with an ultrahigh solvent permeance of 75.3 L m^{-2} h^{-1} bar^{-1} (Figure 2c and **Table 1**). This methanol permeance is 1.5 times higher than that of polyamide nanofilms[3] and 12 times higher than that of a GO membrane.[22,23] A 100% rejection of EB was still maintained even at a high EB concentration (1.0 g L^{-1}) or in a strong acidic solution (0.5 mol L^{-1} hydrochloric acid) (Figure S11, Supporting Information). In a strong acidic medium, the negative charges of EB and S-rGO-18 were extensively neutralized; thus the excellent molecular separation performance should be attributed only to size exclusion. Therefore, it is reasonable to conclude that the nanochannels in S-rGO coating are narrower than the size of an EB molecule (3.4 nm). The rejection values for negatively charged dyes decreased monotonously with

Table 1. The separation performances of S-rGO-18 and HPEI/S-rGO-18 membranes for solutes with different sizes and charges in methanol or water. BF and MB are positively charged, BY and EB are negatively charged; the unit of permeance is L m^{-2} h^{-1} bar^{-1}.

OSN membrane	Solvent	BF (1.6 nm)		MB (2.0 nm)		BY (2.6 nm)		EB (3.4 nm)	
		Perm.[a)]	Rej. [%][a)]	Perm.	Rej. [%]	Perm.	Rej. [%]	Perm.	Rej. [%]
S-rGO-18	Methanol	76.9	≈0	77.2	≈0	76.0	86.2	75.3	100
	Water	91.3	13.1	90.2	12.6	88.3	99.2	87.6	100
HPEI/S-rGO-18	Methanol	74.2	88.5	72.5	90	75.0	≈0	73.6	100
	Water	86.5	97.5	85.4	98.6	87.0	15.0	85.2	100

[a)]Perm.: permeance; Rej.: rejection.

decreasing molecular size of the dyes; for example, 86.2% for brilliant yellow (BY) and 70.1% for acid fuchsin (AF) (Table 1 and Figure S12, Supporting Information). S-rGO-18 membrane showed almost no rejection to positively charged molecules, such as basic fuchsin (BF) and methylene blue (MB) (Table 1). These results indicate that the nanochannels of S-rGO coating are wider than the molecular size of MB (2.0 nm). On the other hand, HPEI functionalized S-rGO-18 composite membranes (HPEI/S-rGO-18, Figure S13, Supporting Information) exhibited high rejections (≈90%) to positively charged solutes (e.g., BF and MB) in methanol because of its positive surface charges, while its rejection to negatively charged AF molecules were negligible (Table 1 and Figure S14, Supporting Information). Therefore, S-rGO and HPEI/S-rGO membranes can be applied to separate solutes with comparable sizes based on the types of their surface charges. For example, a mixture of AF and MB was separated by using a HPEI/S-rGO-18 membrane (Figure S15, Supporting Information). After filtrating half volume of the feed solution, the concentration of MB in the retentate solution was nearly doubled that in the feed solution, while its concentration in the permeate solution decreased for about 10 times. In contrast, the concentration of AF in the retentate and permeate solutions was nearly the same to that in the feed solution. This function is unique and important because the common size exclusion-based OSN membranes do not have this ability. S-rGO-18 and HPEI/S-rGO-18 membranes also exhibited high permeance and excellent selectivity in water. For the same dye, the rejection value in water was tested to be higher than that in methanol. As shown in Table 1 and Figure S16 (Supporting Information), S-rGO-18 membrane can reject 92.4% AF or 99.2% BY molecules with a water permeance of ≈90 L m^{-2} h^{-1} bar^{-1}. HPEI/S-rGO-18 membrane is able to reject 97.5% BF or 98.6% MB molecules with a water permeance of ≈85 L m^{-2} h^{-1} bar^{-1}. This is mainly due to that the carboxyl or amine groups of these membranes can be ionized or protonated to higher degrees in water than in an organic solvent to generate more charges. Impressively, S-rGO-18 membrane can even reject 85.2% of potassium ferricyanide ($[Fe(CN)_6]^{3-}$, ≈0.95 nm), and HPEI/S-rGO-18 membrane is able to reject 58.3% of $MgCl_2$ (hydrated Mg^{2+}, ≈0.86 nm) in water (Figure S17, Supporting Information).

Durability and mechanical stability are very important for the practical applications of an OSN membrane.[2] The S-rGO coating of an S-rGO-*n* membrane stayed intact upon violent washing or stirring (600 rpm). This is mainly due to that the strong rGO sheets provide the S-rGO coating with a high mechanical strength.[5,6] Furthermore, the rGO sheets on the bottom surface of S-rGO coating were partly embedded into the pores of the underlying Nylon support membrane, greatly enhancing the interfacial interaction of this bilayer composite membrane. This fact has been confirmed by the surface morphology of the rGO coating mechanically detached from its Nylon support (Figure S18, Supporting Information), showing a rough surface imprinted from the micropores of the filtering paper.

Many postreaction mixtures of chemical syntheses contain strong basic, acidic or corrosive components. Thus, OSN membranes with excellent chemical and mechanical stabilities in these harsh environments are highly desirable.[1,2] However, the widely used polymeric OSN membranes are usually deteriorated or even decomposed in these systems (basic, acidic, oxidative).[1,2] Fortunately, our S-rGO-18 composite membrane was found to be intact after soaking in 0.5 M H_2SO_4, 0.5 M KOH, or 0.5 M HNO_3 for at least one day, showing a high solvent permeance and 100% rejection for EB (**Figure 3**a).

Organometallic complexes are widely used as homogeneous catalysts for organic syntheses. They usually have rigid 3D structures carrying with or without electrical charges. The separation and recovery of these expensive catalysts from reaction products is a recurrent problem in homogeneous catalysis.[1,2] Common separation techniques have several disadvantages, including batch-based or discontinuous operation, high energy and solvent consumption, as well as the loss of high-value ligands.[1,2] As illustrated in Figure 3b, these issues can be addressed by combining continuous catalytic process with OSN-assisted catalyst recovery.[25,26] However, currently available OSN membranes usually have low solvent permeances with broad rejection curves; the rejection rate increases gradually with increasing solute size over a wide range of solute sizes. As a result, they can reject not only the large catalyst complexes, but also considerable amounts of reactants or products, lowering operation efficiencies.[26] In contrast, our S-rGO-*n* membranes are able to exclusively reject large organometallic complexes without blocking small reactants and products. As a demonstration, we tested the rejection performance of HPEI/S-rGO-18 membrane for BINAP-Ru(II) complexes (BINAP = 2, 2′-bis(diphenylphosphino)-1, 1′-binaphthyl), a widely used homogenous catalyst for asymmetric hydrogenation.[27] This membrane selectively rejected 98% of positively charged BINAP-Ru(II) complexes with an ultrahigh methanol permeance of 70 L m^{-2} h^{-1} bar^{-1}, while allowed the unimpeded transport of neutral substrate molecules (Figure 3c and Figure S19,

Adv. Mater. **2016**,
DOI: 10.1002/adma.201601606

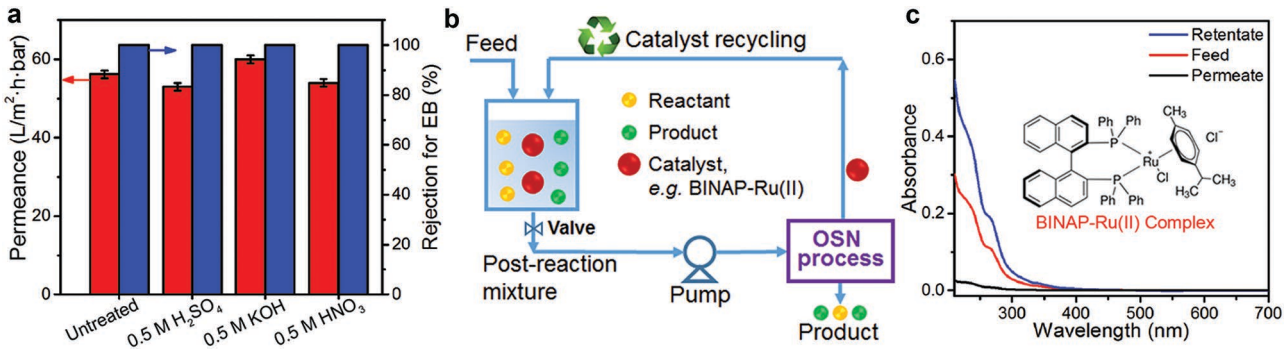

Figure 3. The durability and stability of S-rGO-*n* membranes and a demonstration of catalyst separation. a) The performance comparison of an S-rGO-25 membrane before and after the treatment by immersing in 0.5 M H_2SO_4, 0.5 M KOH, or 0.5 M HNO_3 for one day. b) Schematic illustration of an OSN-assisted catalyst recycling process. c) UV–vis absorption spectra of a methanol solution of BINAP-Ru(II) complex before and after filtration through an HPEI/S-rGO-18 membrane; inset shows the chemical structure of BINAP-Ru(II) complex.

Supporting Information). Furthermore, the chemical structure of BINAP-Ru(II) catalyst kept intact after nanofiltration as confirmed by UV–visible and mass spectral examinations (Figure 3c and Figure S20, Supporting Information).

In summary, we have successfully developed high-performance S-rGO-based OSN membranes. They show high rejections to small molecules with charges the same to that of S-rGO coatings or neutral molecules with sizes larger than 3.4 nm, while retaining their high permeances to organic solvents. Moreover, these OSN membranes are stable in organic solvents, and strong acidic, alkaline, or oxidative media; their performances can be further improved or modulated by modifying with ionic polyelectrolytes, showing great potentials for practical applications.

Experimental Section

Preparation of rGO Dispersion: GO dispersion was prepared from natural graphite powder by a modified Hummers method as described in a previous paper.[14] Then GO dispersion was reduced by hydrazine in an alkaline aqueous medium.[6] Typically, GO dispersion (20 mL, 0.25 mg mL^{-1}) was mixed with hydrazine (7.07 µL, 99 wt%) and ammonia solution (78.4 µL, 25 wt% in water) in a 30 mL glass vial. The mixed dispersion was then vigorously shaken and placed in an oven at 40 °C for 3 h.

Fabrication of S-rGO-n Membranes: S-rGO-*n* membranes were prepared by vacuum filtration of diluted rGO dispersions through Nylon microfilter membranes (47 mm in diameter, 0.65 µm pore size) or anodic aluminum oxide membranes (47 mm in diameter, 0.2 µm pore size). Once the filtration was completed (no free rGO dispersion was left in the filter, but the membrane still remained wet), a certain amount of organic solvent or water was immediately poured on the surface of as-formed S-rGO coating to keep it in solvated state.

Fabrication of HPEI/S-rGO-n Membranes: An as-prepared S-rGO-*n* membrane was soaked in HPEI aqueous solution (0.1 wt%) at room temperature for 30 min and then washed with excessive water. The positively charged HPEI chains were adsorbed onto the negatively charged S-rGO-*n* membrane to switch its surface charges into positive. The zeta potential of HPEI/S-rGO membranes in 1×10^{-3} M KCl solution was determined to be 61.85 ± 1.20 mV.

OSN Performances of S-rGO-n and HPEI/S-rGO-n Membranes: Nanofiltration experiments were carried out using a stirred vacuum filtration setup or a stainless steel dead-end filtration device applicable for high-pressure filtration tests (Figure S7, Supporting Information). The stirring rate of the mechanical agitator was set at 600 rpm. At least two identical samples for each OSN membrane were tested to achieve reliable values of solvent permeances and rejection rates. The area of an S-rGO membrane contacted with the feed solution was 7.07 cm^2 (a round area with a diameter of 3 cm). All the S-rGO composite membranes used for nanofiltration tests were supported by Nylon microfiltration membranes unless specified. An S-rGO-*n* or an HPEI/S-rGO-*n* membrane was first stabilized by filtrating with pure water until a steady water permeance was achieved (Figure S8, Supporting Information). Then the permeances of organic solvents and the rejection for various solutes were measured. Various dyes dissolved in methanol or water were used as molecular markers to determine the selectivity of these membranes. The concentrations of feeding solutions ranged from 2 to 10 mg L^{-1}, depending on the absorbance of the tested dyes. The concentrations of feed, permeate, and retentate solutions were measured by using UV–vis spectrophotometer. The concentration of $MgCl_2$ aqueous solution was calculated according to its ionic conductivity. The concentration of potassium ferricyanide aqueous solution was determined by either using a UV–vis spectrophotometer or an ionic conductivity meter. To exclude the effect of solute adsorption, in all the rejection tests, the rejection rates of solutes were calculated after their concentrations in the permeate solutions became steady. In addition, the mass balance for solutes in the feed, retentate, and permeate solutions was calculated. The results indicated that the total solute mass in the retentate and permeate solutions equaled to the solute mass in the feed solution.

Solvent permeance (F) was calculated using Equation (1)

$$F = V/(A \times t \times \Delta P) \quad (1)$$

where V is the volume of permeate (L), A is the effective membrane area (m^2), t is the permeation time (h), and ΔP is the transmembrane pressure (bar). So the unit of F is L m^{-2} h^{-1} bar^{-1}.

The rejection (R) of markers was calculated using Equation (2)

$$R = (1 - C_P/C_R) \times 100\% \quad (2)$$

where C_P and C_R are the concentrations of markers in the permeate and retentate solutions.

Characterization: SEM images were taken out by the use of a Sirion-200 scanning electron microscope (FEI, USA) with an accelerating voltage of 10 kV. XRD was performed on a D8 Advance X-ray diffractometer with Cu Kα radiation (λ = 0.15418 nm, Bruker, Germany). AFM images were recorded on an SPM 9600 microscope (Shimadzu, Japan). Raman spectra were obtained by the use of a LabRAM HR Evolution (HORIBA Jobin Yvon, France) Raman microscope with a 532 nm laser. XPS spectra were collected by using an ESCALAB 250XI photoelectron spectrometer (ThermoFisher Scientific, USA). UV–vis spectra were carried out on a Lambda 35 spectrophotometer (PerkinElmer, USA). Zeta potential tests were conducted on SurPASS zeta potential analyzer (Anton Paar, Austria) by using standard condition.

Supporting Information

Supporting Information is available from the Wiley Online Library or from the author.

Acknowledgements

This work was supported by the National Basic Research Program of China (2012CB933402, 2013CB933001) and the Natural Science Foundation of China (51433005).

Received: March 23, 2016
Revised: July 13, 2016
Published online:

[1] P. Marchetti, M. F. J. Solomon, G. Szekely, A. G. Livingston, *Chem. Rev.* **2014**, *114*, 10735.
[2] P. Vandezande, L. E. Gevers, I. F. Vankelecom, *Chem. Soc. Rev.* **2008**, *37*, 365.
[3] S. Karan, Z. Jiang, A. G. Livingston, *Science* **2015**, *348*, 1347.
[4] S. Karan, S. Samitsu, X. Peng, K. Kurashima, I. Ichinose, *Science* **2012**, *335*, 444.
[5] C. Gómez-Navarro, J. C. Meyer, R. S. Sundaram, A. Chuvilin, S. Kurasch, M. Burghard, K. Kern, U. Kaiser, *Nano Lett.* **2010**, *10*, 1144.
[6] D. Li, M. B. Müller, S. Gilje, R. B. Kaner, G. G. Wallace, *Nat. Nanotechnol.* **2008**, *3*, 101.
[7] R. K. Joshi, P. Carbone, F. C. Wang, V. G. Kravets, Y. Su, I. V. Grigorieva, H. A. Wu, A. K. Geim, R. R. Nair, *Science* **2014**, *343*, 752.
[8] P. Sun, M. Zhu, K. Wang, M. Zhong, J. Wei, D. Wu, Z. Xu, H. Zhu, *ACS Nano* **2013**, *7*, 428.
[9] K. Raidongia, J. X. Huang, *J. Am. Chem. Soc.* **2012**, *134*, 16528.
[10] B. Mi, *Science* **2014**, *343*, 740.
[11] K. Huang, G. Liu, J. Shen, Z. Chu, H. Zhou, X. Gu, W. Jin, N. Xu, *Adv. Funct. Mater.* **2015**, *25*, 5809.
[12] G. Liu, W. Jin, N. Xu, *Chem. Soc. Rev.* **2015**, *44*, 5016.
[13] B. Yao, J. Chen, L. Huang, Q. Zhou, G. Shi, *Adv. Mater.* **2016**, *28*, 1623.
[14] L. Huang, Y. Li, Q. Zhou, W. Yuan, G. Shi, *Adv. Mater.* **2015**, *27*, 3797.
[15] H. Huang, Z. Song, N. Wei, L. Shi, Y. Mao, Y. Ying, L. Sun, Z. Xu, X. Peng, *Nat. Commun.* **2013**, *4*, 2979.
[16] D. Cohen-Tanugi, J. C. Grossman, *Nano Lett.* **2012**, *12*, 3602.
[17] Y. Han, Z. Xu, C. Gao, *Adv. Funct. Mater.* **2013**, *23*, 3693.
[18] M. Hu, B. Mi, *Environ. Sci. Technol.* **2013**, *47*, 3715.
[19] L. Qiu, X. Zhang, W. Yang, Y. Wang, G. P. Simon, D. Li, *Chem. Commun.* **2011**, *47*, 5810.
[20] Y. Wang, S. Chen, L. Qiu, K. Wang, H. Wang, G. P. Simon, D. Li, *Adv. Funct. Mater.* **2015**, *25*, 126.
[21] Y. Zhang, S. Zhang, T. S. Chung, *Environ. Sci. Technol.* **2015**, *49*, 10235.
[22] N. F. D. Aba, J. Y. Chong, B. Wang, C. Mattevi, K. Li, *J. Membr. Sci.* **2015**, *484*, 87.
[23] J. Y. Chong, N. F. Aba, B. Wang, C. Mattevi, K. Li, *Sci. Rep.* **2015**, *5*, 15799.
[24] J. W. S. Hummers, R. E. Offeman, *J. Am. Chem. Soc.* **1958**, *80*, 1339.
[25] K. De Smet, S. Aerts, E. Ceulemans, I. F. J. Vankelecom, P. A. Jacobs, *Chem. Commun.* **2001**, *2001*, 597.
[26] D. Nair, H. T. Wong, S. Han, I. F. J. Vankelecom, L. S. White, A. G. Livingston, A. T. Boam, *Org. Process Res. Dev.* **2009**, *13*, 863.
[27] R. Noyori, H. Takaya, *Acc. Chem. Res.* **1990**, *23*, 345.